

# Compression characteristics of filling gangue and simulation of mining with gangue backfilling: An experimental investigation

Changxiang Wang<sup>1,2a</sup>, Baotang Shen<sup>1,2</sup>, Juntao Chen<sup>\*1,2</sup>, Weixin Tong<sup>1,2</sup>,  
Zhe Jiang<sup>1,2</sup>, Yin Liu<sup>1,2</sup> and Yangyang Li<sup>1,2</sup>

<sup>1</sup>College of Mining and Safety Engineering, Shandong University of Science and Technology, Qingdao 266590, China

<sup>2</sup>State Key Laboratory of Mining Disaster Prevention and Control Co-Founded by Shandong Province and the Ministry of Science and Technology, Shandong University of Science and Technology, Qingdao 266590, China

(Received November 16, 2019, Revised February 10, 2020, Accepted February 17, 2020)

**Abstract.** Based on the movement characteristics of overlying strata with gangue backfilling, the compression test of gangue is designed. The deformation characteristics of gangue is obtained based on the different Talbot index. The deformation has a logarithmic growth trend, including sharp deformation stage, linear deformation stage, rheological stage, and the resistance to deformation changes in different stages. The more advantageous Talbot gradation index is obtained to control the surface subsidence. On the basis of similarity simulation test with gangue backfilling, the characteristics of roof failure and the evolution of the supporting force are analyzed. In the early stage of gangue backfilling, beam structure damage directly occurs at the roof, and the layer is separated from the overlying rock. As the working face advances, the crack arch of the basic roof is generated, and the separation layer is closed. Due to the supporting effect of filling gangue, the stress concentration in gangue backfilling stope is relatively mild. Based on the equivalent mining height model of gangue backfilling stope, the relationship between full ratio and mining height is obtained. It is necessary to ensure that the gradation of filling gangue meets the Talbot distribution of  $n=0.5$ , and the full ratio meets the protection grade requirements of surface buildings.

**Keywords:** mining under village; compression test of filling gangue; Talbot gradation index; gangue backfilling similarity simulation test; full ratio

## 1. Introduction

China is a large energy producer and consumer of coal resources. Due to the pursuit of short-term economic benefits and inadequate attention to environmental protection of coal mine, environmental pollution and degradation have occurred in recent years (Zhang *et al.* 2019, Li *et al.* 2018). Land deterioration, water resources pollution and air pollution caused by coal gangue spontaneous combustion have resulted in three-dimensional harm to human living environment (Wang *et al.* 2019, Muriithi *et al.* 2017, Guo *et al.* 2019a, b). In addition, the shortage of coal reserve resources and the potential risk of coal mining under village are increasingly prominent (Yin *et al.* 2018, Zhang *et al.* 2016).

Gangue is the solid waste discharged from coal mining and washing process and it is imperative to reduce the mining-induced hazards and gangue pollution (Ma *et al.* 2018, 2017, Sun *et al.* 2019). Due to the environmental, social and economic benefit, filling with coal gangue has been emphasized in coal mining. The filling gangue can fill the coal goaf, form the supporting structure and change

the movement mode of the overlying strata. Coal gangue filling has been conducted under the large-scale buildings, the railroad and the water body with significant economic, social and environmental benefits (Wang *et al.* 2019, 2011).

Plenty of studies have been carried out on the compaction behavior of the gangue by experimental (Ghabchi *et al.* 2014, Indraratna and Locke 1999) and numerical methods (Poulsen *et al.* 2013, Chen *et al.* 2019). Many studies revealed that the phenomenon of gangue breakage is often accompanied by the occurrence of rock gangues compaction, and significant experimental methods were conducted to analyze the gangue crushing behavior, such as acoustic emission patterns (Li *et al.* 2018, Liu *et al.* 2019) and gangue gradation (Marcin *et al.* 2016, Casini *et al.* 2013). During the compression process of filling gangue, deformation of filling gangue can be affected by environmental factors, such as the overlying strata load, the later construction load, and the influence of groundwater or atmospheric precipitation (Gu *et al.* 2018, Hu *et al.* 2018, Shahriar *et al.* 2015). Correlation studies also show that particle crushing is related to particle strength (Rozenblat *et al.* 2011, Coop *et al.* 2004, Zhao *et al.* 2018, Zhao *et al.* 2019), loading mode (Friedemann *et al.* 2016, Donohue *et al.* 2009, Vogler *et al.* 2016).

During the gangue filling process, the large gangue should be crushed. Since the raw gangue has natural defects with discontinuous gradation in the field, raw gangue should be manually broken into a specific particle size to guarantee filling effect. However, the specific particle size

\*Corresponding author, Ph.D.

E-mail: polariscjt@126.com

<sup>a</sup>Ph.D. Candidate

E-mail: 1554624100@qq.com

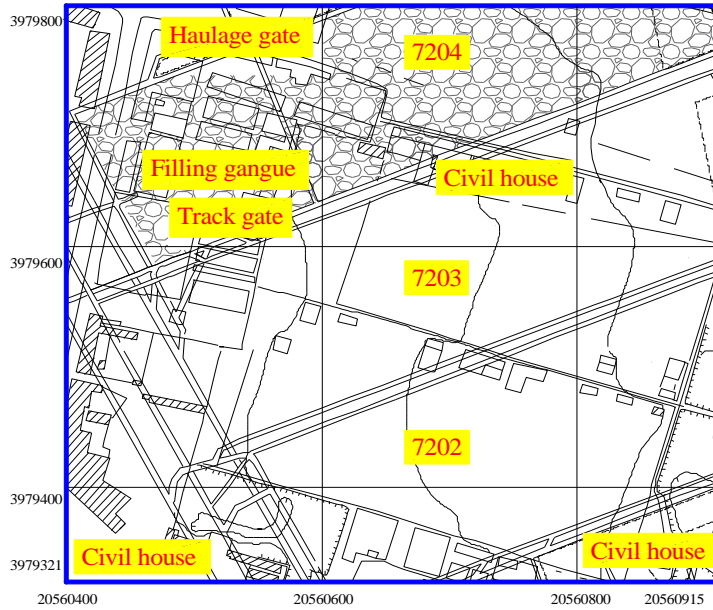


Fig. 1 Layout of the mining system (adapted from Guo 2013)

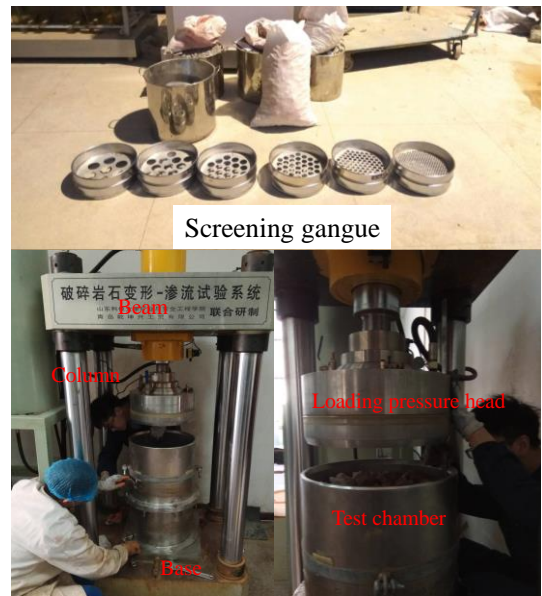
is not explored clear. And it is also an urgent problem that how to satisfy the protection grade of different buildings through gangue filling. To this end, the deformation characteristics of filling gangue and the movement mode of overburden rock after gangue filling are investigated under the engineering background of gangue filling in a fully mechanized mining face. Besides, the supporting system of gangue filling and the evolution law of mechanical relationship between filling gangue and surrounding rock are analyzed theoretically. Finally, the equivalent mining height model and full ratio of gangue filling are developed and effectively applied to the field application.

The studied coal mine area is located in Tai'an City, Shandong Province. In order to overcome the serious problems, such as the coal excavation under village, auxiliary lifting and ground gangue accumulation, gangue filling mining has been used in No.7204 working face. The coal seam thickness of No.7204 working face is 2.0 m with the stable coal seam. Fig. 1 shows the working face layout. The average depth from the working face to the ground is about 500m. The lithology of the roof and floor is mainly sandstone. The overlying surface of the south wing of the mining area is a village, and the north has buildings of schools, hospitals, towns, etc., as shown in Fig. 1 (Guo 2013).

**2. Compression test of filling gangue**

*2.1 Experimental systems*

The experimental control system consists of a console and a servo loading system. The whole process is automatically controlled by the computer, experimental loading and unloading system and experimental preparation process, as shown in Fig. 2. The relevant technical parameters are shown in Table 1.



Assembly instrument Initial measurement  
Fig. 2 System and experimental preparation process

Table 1 Major parameters of experimental system

Axial compression	≤600 kN	Accuracy	0.01 kN
Displacement of hydraulic cylinder	≤500 mm	Accuracy	0.01 mm
Diameter of the test chamber	400 mm	Height	680 mm

*2.2 Experimental schemes*

*2.2.1 Loading mode*

The early overburden acting on the filling gangue is mainly related to the movement space of the overburden in addition to its lithology. According to the overburden movement, the force of the early overburden on the backfill materials can be estimated by

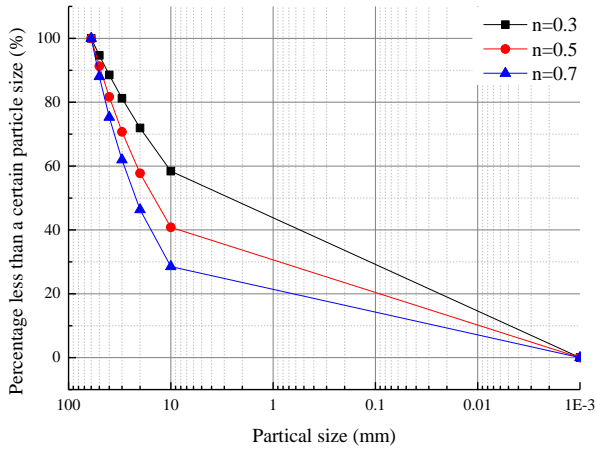


Fig. 3 Particle size distribution of different gradation indices

Table 2 Particle size distribution of different gradation index

Talbot index	Particle/mm	0~10	10~20	20~30	30~40	40~50	50~60
n=0.3	Pass rate before test P/%	58.42	13.50	9.31	7.32	6.13	5.32
	Pass rate after test P/%	65.02	16.32	8.78	6.75	2.11	1.02
n=0.5	Pass rate before test P/%	40.82	16.91	12.98	10.94	9.64	8.71
	Pass rate after test P/%	60.02	19.89	9.02	7.53	2.53	1.01
n=0.7	Pass rate before test P/%	28.53	17.82	15.61	13.33	12.73	11.98
	Pass rate after test P/%	47.14	23.82	18.32	6.85	2.35	1.52

$$\sigma_z = \frac{\gamma h}{K_A - 1} \quad (1)$$

where  $h$  is the overlying motion space, namely the unfilled space, and  $h$  is assumed as 0.5 m;  $\gamma$  is the overburden bulk density,  $\gamma = 25 \text{ kN/m}^3$ ;  $K_A$  is breaking expansion coefficient of partial caving overburden,  $K_A$  ranges from 1.2~1.25 in line with the previous experience.

Therefore, the early overburden force on the backfill can be simplified as follows:

$$\sigma_z = (4 \sim 5)\gamma h \quad (2)$$

The calculated load on the filling gangue is about 0.06 MPa, and the late load is about 0.6 MPa according to the previous experience (State Bureau of Coal Industry 2017). So the diameter of the test chamber is 400 mm with the maximum load of 100 kN. When filling the goaf with gangue, the force on the gangue will increase linearly until it equals to the gravity of overlying strata in water-conducting zone. The axial load is increased to 100 kN by

0.5kN/s loading rate. When the axial load reached 100kN, it is maintained for about 5.5h.

### 2.2.2 Fractured rock particle size gradation

Talbot index (An Talbot *et al.* 1923) has important implications for the design of material proportion. The Talbot formula is defined as:

$$p = 100 \left( \frac{d}{D} \right)^n \quad (3)$$

where  $p$  is the pass percentage of particles with the radius smaller than  $d$ ;  $D$  is the maximum grain size of the material;  $n$  is gradation index.

Results show that, in the Talbot's grading, gangue samples have a higher deformation modulus than fully graded and single-graded gangue samples (Li *et al.* 2016, Guida *et al.* 2016). The maximum particle size is 60 mm according to field application requirements, the large blocks of fractured gangues are crushed and sieved into a total of 6 particle size interval, including 0~10 mm, 10~20 mm, 20~30 mm, 30~40 mm, 40~50 mm and 50~60 mm by the grading. The total mass is 110 kg.

To obtain the effect of different gradation index on the compression of broken gangue, the compression test was carried out with  $n=0.3, 0.5, 0.7$ . The particle size distribution is shown in Fig. 3 and Table 2.

### 2.2.3 Initial dilatation characteristics

The dilatancy of rock indicates that the rock volume after the breakage can increase compared with the intact rock volume. It is usually expressed by the dilatation coefficient or porosity, and calculated by:

$$K = \frac{V_1}{V_0} \quad (4)$$

$$P = \frac{V_1 - V_0}{V_1} \times 100\% = 1 - \frac{1}{K} \quad (5)$$

where  $K$  is the dilatation coefficient;  $V_0$  is the volume of an intact rock block;  $V_1$  is the volume of the intact rock block after the breakage;  $P$  is the porosity.

The broken rock used in the test is sandstone, the density of the intact rock is  $2.54 \text{ g/cm}^3$ . The volume of broken rock is converted to that of intact rock in the test chamber, namely  $V_0=0.04331 \text{ m}^3$ . When  $n=0.3$ , the mass of broken rock with different particle sizes is mixed into the test chamber. The height of the broken rock in the test chamber is 628 mm and the total volume is  $0.07892 \text{ m}^3$ , namely  $V_1=0.07892 \text{ m}^3$ ;  $n=0.3$ . Therefore, if  $n=0.3$ , the initial dilatancy coefficient of broken rock  $K=1.82$ , and the porosity  $P=0.45$ ; if  $n=0.5$ , then  $K=1.74$  and  $P=0.42$ ; if  $n=0.7$ , then  $K=1.83$  and  $P=0.45$ .

Obviously, with the increase of gradation index from 0.3, 0.5 and 0.7, the initial dilatation coefficient of broken gangue goes first decreases and then increases, namely when  $n=0.5$ , the initial dilatation coefficient of broken gangue is the smallest and the structure of broken gangue is more reasonable at this time.

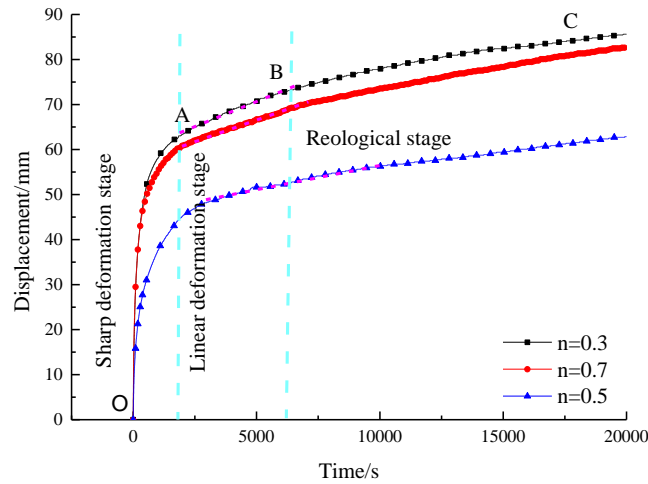


Fig. 4 Gangue compression deformation curve

Table 3 Variable gradation index for each stage deformation parameter

$n$	H/mm	OC		OA			AB			BC		
		Dis/mm	Strain	Dis/mm	Strain	Ratio/%	Dis/mm	Strain	Ratio/%	Dis/mm	Strain	Ratio/%
0.3	628	85	0.14	63	0.10	74	9	0.01	10	13	0.02	15
0.5	601	61	0.10	47	0.08	77	4	0.01	7	10	0.02	16
0.7	631	82	0.13	59	0.09	72	8	0.01	10	15	0.02	18

Dis: displacement; H: height before compression. Ratio: percentage of displacement change at different stages

### 2.3 Experimental results

The displacement-time curve is obtained from the experiment, as shown in Fig. 4. It can be clearly seen that the displacement-time relationship curve of different gradation indexes have a similar trend. The displacement-time curve of  $n=0.3$  is close to that of  $n=0.7$ . When  $n=0.5$ , the displacement-time curve is below the curves of  $n=0.3$  and  $n=0.7$ . Table 3 and Fig. 5 show deformation parameters of each stage. With the increase of gradation index, the corresponding deformation parameters decrease first and then increase, namely the corresponding deformation parameters are the smallest if  $n=0.5$ . It can be concluded that if  $n=0.5$ , the filling gangue has the smaller initial void and stronger resistance to deformation. Therefore, when large gangue is broken, the filling effect can be improved if the Talbot distribution of  $n=0.5$  is ensured for the gradation of filling gangue after crushing in engineering application. In the compression process of gangue, there are three stages of gangue deformation, namely, sharp deformation stage OA, linear deformation stage AB, rheological stage BC. As shown in Figs. 5 and 6, when  $n=0.5$ , the original height of filling gangue is 601mm, and the total value of deformation is 61 mm after loading 5.5 h. The first stage is the OA section, namely the sharp deformation stage, as the load increases to the constant value, the deformation of the filling gangue increases sharply. The deformation value is 47 mm, the deformation rate is 77% and the strain is 0.08. The second stage is the AB section, namely the linear deformation stage. The curve approximates a straight line, indicating that the slope of the curve tends to be constant,

the deformation value is 4mm, the deformation rate is 7% and the strain is 0.01. There is no obvious decrease in deformation rate, indicating that the resistance to deformation of crushing gangue and the particle gradation of natural gangue are not changed obviously. The third stage is the BC stage, namely the rheological stage. At this point, the deformation value is 10 mm, the deformation rate is 16% and the strain is 0.02. As the filling gangue is compacted continuously, the edges and corners of some particles are crushed gradually. At this time, there is an obvious nonlinear relationship between time and compression ratio, the deformation rate decreases gradually, and the resistance to deformation is obviously enhanced. The decrease of deformation rate indicates that the particle gradation defects of natural gangue can be improved effectively during the compaction.

The above analysis is based on the loading time of 5.5 h. If the loading time is long enough, the dilatation coefficient is infinitely close to 1, and the ultimate deformation value is 253.63 mm and the ultimate strain is 0.43. It can be seen that filling gangue compression is a long and slow process. To ensure the filling effect, the optimal gradation and the most economical ultimate strain should be guaranteed.

The particle size distribution after compression experiments of different gradation indexes is shown in Fig. 7 and Table 3. The overall trend is that the proportion of large gangue particles decreases and the proportion of small gangue particles increases. When  $n=0.3$  and  $n=0.7$ , the initial dilatancy coefficient and deformation parameter are similar, while the particle size gradation is not similar after the test. It is referred that the effect of the primary particle

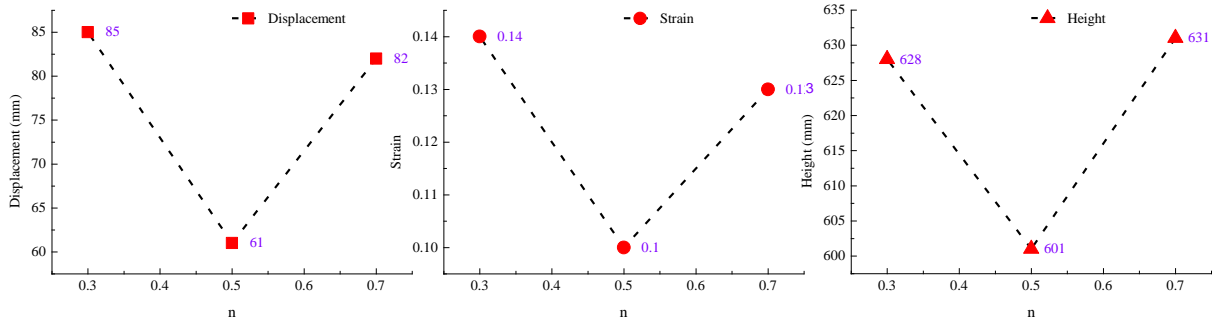


Fig. 5 Variation of deformation parameters in different stages of different gradation indices

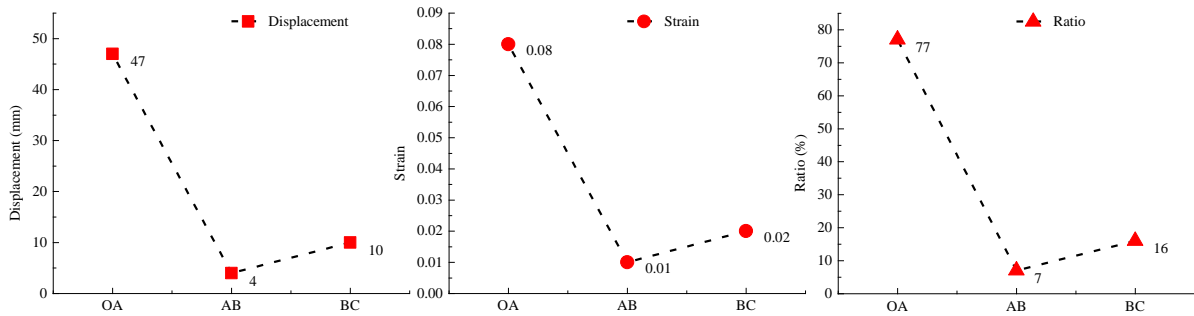


Fig. 6 Deformation parameters at different stages when  $n=0.5$

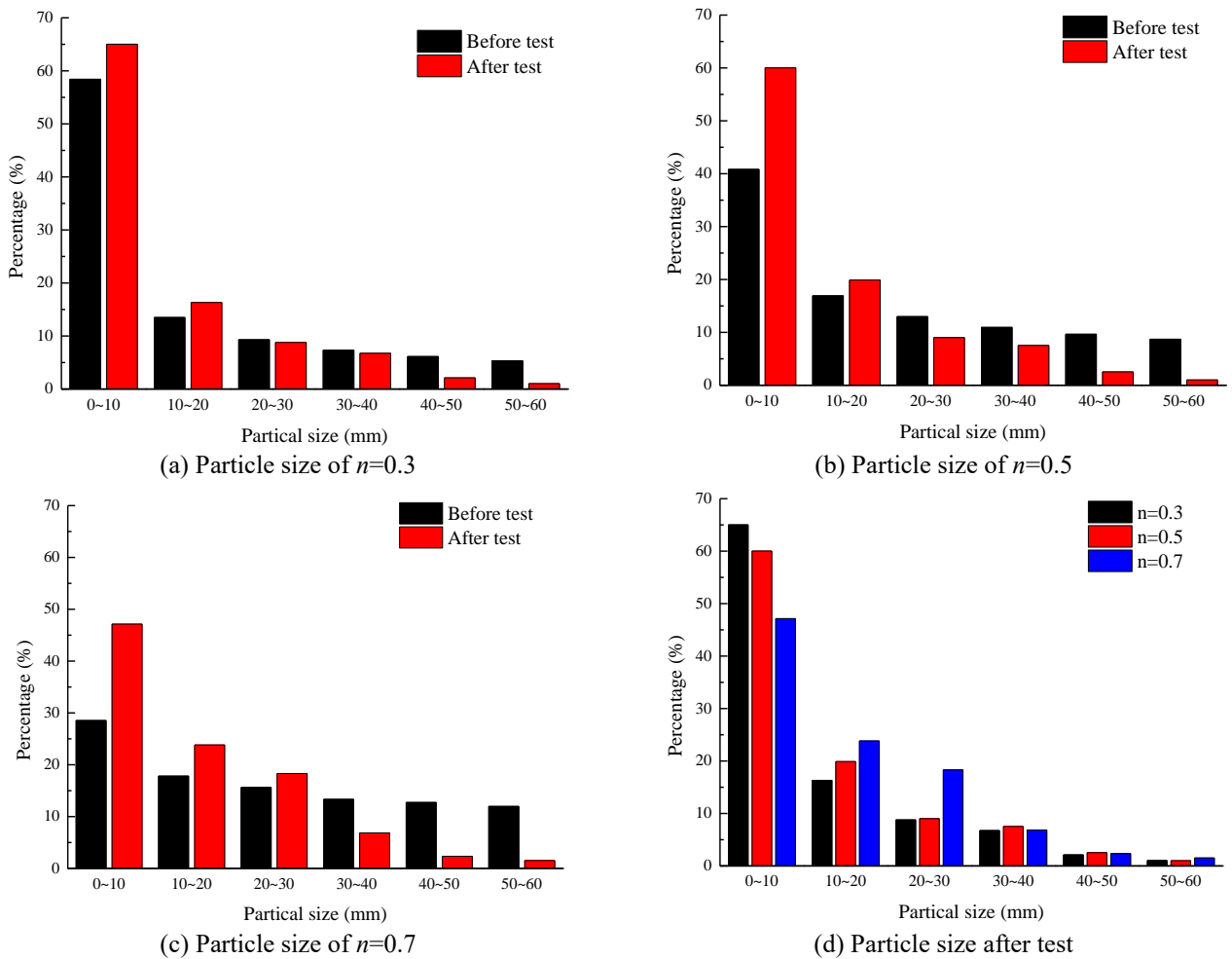


Fig. 7 Particle size change

Columnar section	Thickness/ m	Rock name	Lithological description
	7.0~13.0 9.0	Fine sandstone	Grayish white, layer with black siltstone strip
	5.0~9.0 6.6	Siltstone	Grayish black, containing fossilized plant debris, massive structure
	5.0~11.0 7.0	Sandstone	Broken, fissure development, low mechanical strength
	1.8~2.2 2.0	Mudstone	Gray-black, shale structure, thin layered structure, staggered fracture.
	0.9~2.3 2.0	No.7 coal	Black, crack development, low mechanical properties.
	7.5~14.0 10.5	Siltstone	Gray, dense, with diamonds, with discontinuous wavy horizontal bedding

Fig. 8 The characteristics of the rock formation

size gradation results in the different results under the same lithology and the loading mode.

Fine particles, especially the particles between 0-10 mm, can fill the voids between coarse particles and interact with the larger particles in broken gangue. This phenomenon can be clearly observed during the process of dismantling the test chamber after the experiment. To obtain the comprehensive economic and technical benefits, a certain proportion of fine particles (about 60%) should be maintained in the field filling from the particle size gradation after compaction if  $n=0.5$ .

The gradation of original gangue has natural defects, discontinuous, small particle of gangue has a low ratio. In the actual filling process, the large gangue needs to be broken, which can control the particle size of the secondary crushing, make the improved filling gangue gradation conform to or close to the gradation in this paper, and improve the supporting effect of filling gangue.

The resistance to the roof cannot be generated in the sharp deformation stage of filling gangue. In the linear deformation stage, the filling gangue can effectively support the surrounding rock or pillar, namely the filling gangue has a certain bearing capacity after the volume compression of the gangue is more than 10%. In the rheological stage, more than 13% volume compression of the filling gangue should be performed in the experiments. The filling gangue can be regarded as a dense entirety with the surrounding rock, and the resistance to the deformation of the surrounding rock is large in the stope. In the field application, the filling gangue needs to be precompacted and 10% volume compression should be conducted as the compaction standard.

### 3. Similarity simulation tests of gangue filling

#### 3.1 Experimental schemes

The coal-bearing strata in this mine belong to the Carboniferous, and the upper part of the coal-bearing strata is covered by red clay sandstone, red sandstone and conglomerate. The strike length of 7204 is 570~663 m and the tilt length is 50~138 m. The occurrence information of roof and floor in the 7204 mining area is shown in Fig. 8.

To capture the realistic behaviour of a rock mass via physical modelling techniques, physical models should be developed in accordance with the principles of similarity

Table 4 Model material ratio and laying level

Lithology	Material ratio
Siltite	7:5:5
Fine sandstone	7:8:2
Mudstone	8:6:4
Sandstone	7:7:3
Coal	8:6:4

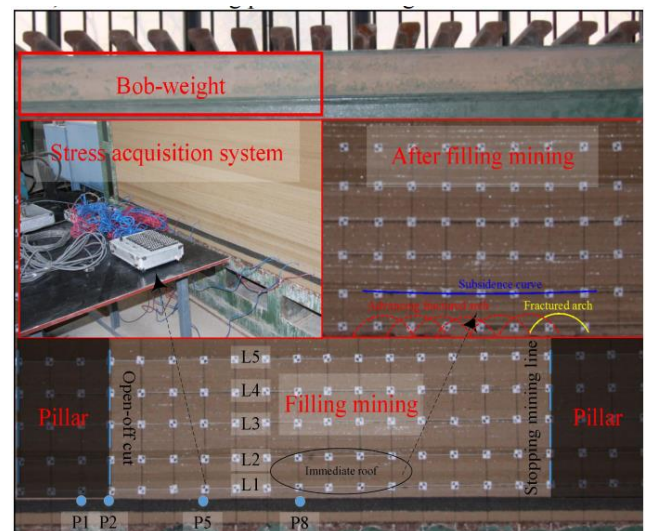


Fig. 9 similarity simulation test of gangue filling

theory (Gu 1995). Since the roof failure range of gangue filling is relatively small, the geometric similarity coefficient of this test model is selected as 1: 50, the bulk density similarity coefficient is 1: 1.5. According to field data of prototype coal and rock strata, sand is used as an aggregate and fly ash and gypsum are used as bonding materials in the model. The material ratio is shown in Table 4 (Gu 1995). The doses of sand, fly ash and gypsum were calculated according to the size and thickness of the model. The laying height is 145 cm, the length is 300 cm, and the width is 40 cm.

According to the stratigraphic condition of gangue filling face, the similarity simulation model is developed by conventional method. The stress is compensated by bob-weight, the coal seam is laid for 4 cm, the coal seam is replaced by board to simulate the gangue filling, the height of board is 3 cm, the compressibility is almost 0, the

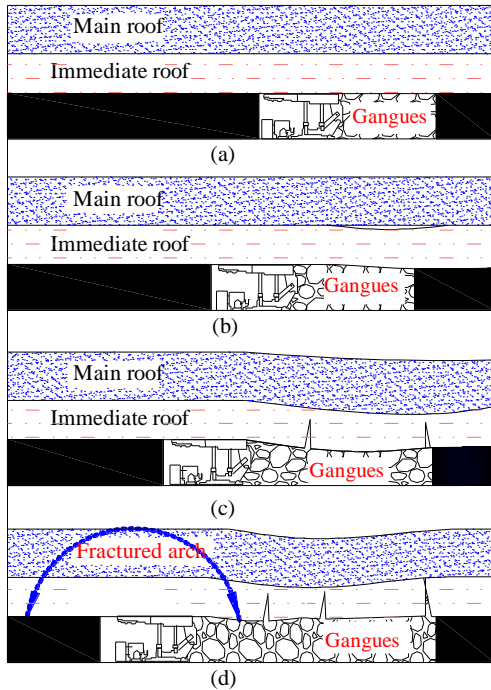


Fig. 10 Overlying rock movement model of gangue filling stope (adapted from Zhang 2017)

advancing length is 140 cm. Fig. 9 shows the model after mining.

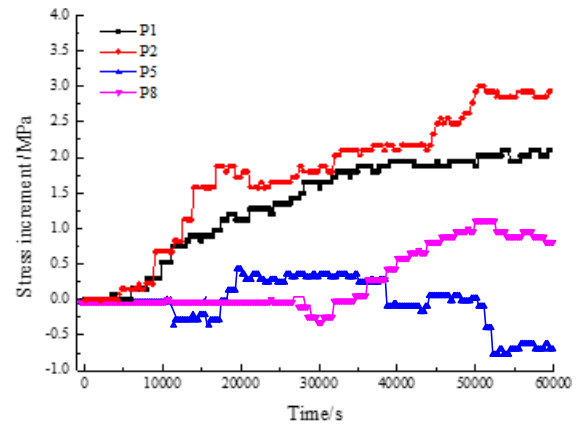
To observe the subsidence of rock strata, the weft lines are placed on the front of the model with ink lines. The mesh line size is 10cm\*10 cm. A total of 10 displacement observation lines are arranged in the upper part of the coal seam. From the bottom up, L1, L2...L10 are arranged in turn, and 20 measuring points are arranged for each line.

Fig. 9 shows the layout scheme. Measuring points are arranged on the floor to monitor the stress evolution. 17 sensors are arranged with the interval of 10cm. The first sensor is set in the pillar and 10 cm away from the open-cut off, and the last sensor is also set in the pillar and 10 cm from the terminal mining line. The stress acquisition system is used for the simulation based on BWL stress sensor, data acquisition box, computer and other equipment, as shown in Fig. 9.

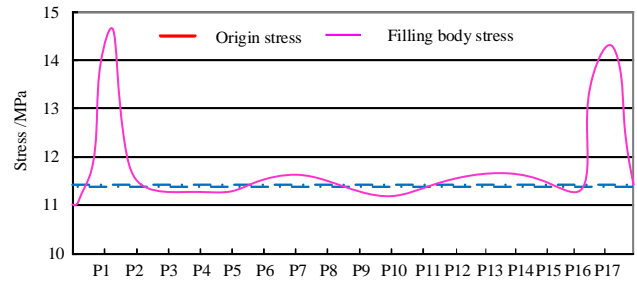
### 3.2 Experimental results

#### 3.2.1 Overburden failure in gangue filling

Fig. 10 shows the failure of overlying strata after filling mining. According to the monitoring results of the displacement, the affected strata are between L1 and L3; the strata between L3 and L2 are obviously separated and subsided; and the strata between L1 and L2, in particular, the direct roof damage is more serious. Fig. 10 shows the process of overlying rock movement. In the early stage of mining and filling, as shown in Fig. 10(a), there is almost no damage to the rock layer, the stress state of rock beam before the first weighting of direct top can be regarded as the fracture of embedded beam. As shown in Fig. 10(b), with the mining and filling gradually advances, layers are separated in the direct roof. As shown in Fig. 10(c), when



(a) Stress increment with time



(b) Stress state after mining

Fig. 11 Stress evolution curve of measuring points

the first weighting is conducted to the direct top, the layer separation is closed, while the mine pressure is weakened. With the further mining, there is the periodic pressure with time for the direct roof, as shown in Fig. 10(d). The periodic pressure is regarded as the periodic fracture of the cantilever beam, and the mine pressure is also weakened.

When the roof contacts the filling gangue behind the working face, a fractured arch of the overburden rock is formed above the working face. Besides, there are micro and macroscopic cracks in the arch of the rock strata and the fractured arch moves forward as the face moves forward, as shown in Figs. 9 and 10 (Zhang 2017).

#### 3.2.2 Supporting stress evolution law in gangue filling

As shown in Figs. 9 and 10, the overburden structure is supported by the supporting system of “coal wall, hydraulic support and filling gangue” in the mining and filling process. Since the overburden structure is an arched structure, and the arch foundation is located in the area in front of the coal wall and the other end is located in the goaf where the stress increased, so the hydraulic support to the overburden structure is very small. The stress of filling gangue at the back of goaf can be restored to the original stress of the rock, indicating that there is an obvious supporting effect. Thus, the range and peak value of the stress concentration area are reduced around the goaf.

To obtain the evolution law of supporting stress in gangue filling face, the data of partial stress sensor are analyzed from the four selected sensors, including P1 (10 cm from the open-off cut within pillar), P2 (in the open-off cut), P5 (30 cm to the open-off cut), and P8 (60 cm to the open-off cut), as shown in Fig. 9. As shown in Fig. 11(a), as

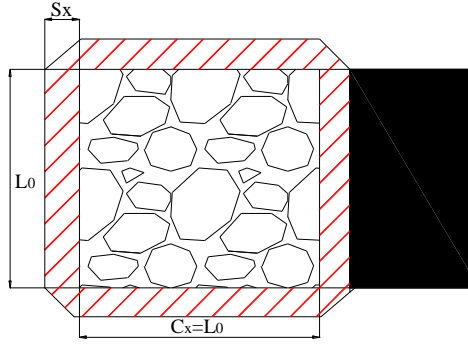


Fig. 12 Stress concentration area around the goaf when the stope is square

the working face moves forward, the stress increment of P1 and P2 increases, indicating that there is the concentrated stress in the pillar. As the working face advancing, the stress of P5 and P8 are first relieved and negative growth occurs. However, when the working face advances over P5 and P8, the trend of stress changes is different, the stress of P5 drops again after rising, the stress of P8 continue rising. The above data shows that in filling the stope, the stress may be concentrated or may fall. At the coal pillar, the stress is definitely concentrated. The stress state after mining also prove this point, as shown in Fig. 11(b). According to the calculation, the stress concentration factor can be obtained as 1.26.

The influence range of the stress concentration area around the goaf reaches the maximum when the advancing distance equals to the width of working face. As the working face continues to advance, the influence range of the stress concentration area around the goaf remains basically unchanged. The model is built as shown in Fig. 12.

As shown in Fig. 12, when the advance distance reaches the working face width, the overlying strata under the gravity stress can form a stress concentration area with width  $S_x$  around the stope. When the bearing capacity of caving gangue is ignored in goaf, the equation for stope stress balance can be expressed as follows:

$$(2L_0 \cdot S_x + 2C_x \cdot S_x + 2 \cdot S_x^2) \cdot (K_a - 1) \cdot \gamma \cdot H = L_0 \cdot C_x \Big|_{=L_0} \cdot \gamma \cdot H - \frac{4}{3} \pi H_g^3 \cdot \gamma_g \quad (6)$$

where  $C_x$  is the advance distance for working face, m;  $L_0$  is the width of working face, m;  $H$  is the buried depth;  $H_g$  is the height of “stress arch”, when the stope advance distance reaches the working face width, then  $H_g = \frac{1}{2} L_0$ ;  $\gamma$  is the overburden bulk density;  $S_x$  is the distribution range of stress concentration area around the goaf;  $K_a$  is the average of stress concentration factors (Kratzsch 1983, An *et al.* 2016).

Eq. (6) can be simplified as:

$$K_a = \frac{L_0 \cdot C_x - \frac{4}{3} \pi \cdot H_g^3}{2L_0 \cdot S_x + 2C_x \cdot S_x + 2 \cdot S_x^2} + 1 \quad (7)$$

During the gangue backfilling, assuming, due to the supporting pressure of gangue filling, the average stress concentration factor is expressed as:

$$K_a = \frac{L_0 \cdot C_x - \frac{4}{3} \pi \cdot H_g^3}{2L_0 \cdot S_x + 2C_x \cdot S_x + 2 \cdot S_x^2 + L_0 \cdot C_x} + 1 \quad (8)$$

where  $H_g$  is the height of “stress arch” of the gangue backfilling.

Since the supporting stress is shared by filling gangue, stress concentration caused by the failure range of mining is greatly reduced. Therefore, the average value of stress concentration factor is reduced obviously.

Suppose there's a work surface,  $C_x=200$  m,  $L_0=200$  m,  $H=500$  m,  $H_g=10$  m,  $S_x=20$  m, Through Eq. (8) to get  $K_a=1.34$ , slightly larger than the experimental data, and the difference is small.

## 4. Full ratio of gangue filling

### 4.1 Concept of full ratio

As shown in Fig. 13, the surface subsidence of gangue filling mining can be predicted by caving mining method based on equivalent mining height ( $M_c$ ). The equivalent mining height is related to the roof subsidence before filling and non-filling account and the compression of the filling gangue (Guo *et al.* 2014, Karacan *et al.* 2010).

$$M_c = S_1 + S_2 + S_3 \quad (9)$$

where  $S_1$  is the roof subsidence before filling;  $S_2$  is non-filling account;  $S_3$  is the compression of the filling gangue. From the geometric relationship, it is concluded that:

$$S_3 = (M - S_1 - S_2) \varepsilon \quad (10)$$

where  $M$  is the actual mining height;  $\varepsilon$  is the strain of filling gangue.

The equation of equivalent mining height can be obtained from the above analysis.

$$M_c = (S_1 + S_2)(1 - \varepsilon) + M \varepsilon \quad (11)$$

After the simple calculation, the full ratio  $F$  value is proposed as:

$$M_c = M(1 - F) \quad (12)$$

$$F = \frac{(M - S_1 - S_2)(1 - \varepsilon)}{M} \quad (13)$$

The full ratio is the essential factor for the measurement of the filling effect. The effective control of the full ratio is vital for the control of the surface subsidence.

### 4.2 Application of full ratio

According to the probability integration method under

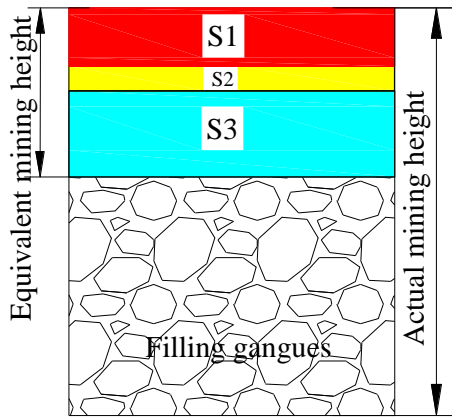


Fig. 13 Equivalent height diagram (adapted from Guo *et al.* 2014)

sufficient mining conditions, three allowable mining heights can be calculated separately (State Administration of Coal Industry 2017), the maximum allowable mining height under the building is:

$$M'_c = \min(M_\xi, M_k, M_i) \quad (14)$$

where  $M_\xi$ ,  $M_k$ ,  $M_i$  are the allowable mining height designed by the maximum allowable surface horizontal deformation, curvature and tilt separately.

To realize the filling effect, it is required that  $M_c \leq M'_c$ , namely the full ratio:

$$F \geq \frac{M - M'_c}{M} \quad (15)$$

The safe mining under the village requires that the most serious damage affected by underground mining can be controlled within damage range of class I. Based on the geological conditions of coal gangue filling face and previous observation of surface rock movement,  $M'_c = 1259$  mm,  $F \geq 0.37$  are calculated by Eqs. (13), (14) and (15). According to the field monitoring,  $S_1 = 112.6$  mm,  $S_2 = 60$  mm, therefore  $\epsilon = 0.60$  is calculated by Eq. (13). The compression ultimate strain of filling gangue is 43% from the compression test in section 2. Therefore, the surface subsidence is effectively controlled.

### 5. Discussion

In this paper, as shown in Fig. 14, the optimal gradation and index of precompaction are obtained by broken rock compression test, and overburden failure mode and index of precompaction during the process of gangue filling is obtained by similarity simulation test. On this basis, the concept of full ratio and ultimate strain are put forward.

From the analysis of the test data, the field compaction procedure for gangue filling is suggested and presented by the following aspects:

*Material selection:*

- 1) Through the gangue compression test with different

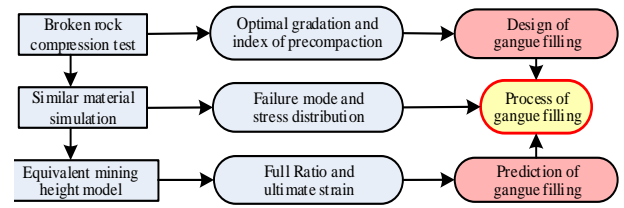


Fig. 14 Connections among broken rock compression test, similarity simulation test and field application

Talbot gradation index, the gradation parameters with the best deformation resistance effect are obtained, and the gangue deformation and strain in different compression stages are further obtained. These data can be used for gangue filling gradation design and the precompaction design of gangue filling.

*Precompaction index:*

- 2) At present, precompacted gangue is used to improve the filling effect in the process of gangue filling. However, it is not very comprehensive to judge the compaction effect by compaction stress. From the experimental results, it can be judged that when the strain of the filling material is 10%, the bearing effect of the filling body against the continuous deformation of the roof rock mass will gradually appear.

*Field execution:*

- 3) Full ratio of gangue filling is far less than filling rate because of its obvious deformation, filling rate can not fully meet the requirements of controlling surface subsidence and protecting surface buildings, so it is necessary to consider the full ratio at this time. Under the condition of ensuring the ultimate strain of filling gangue, the surface deformation is still in the reliable range.

### 6. Conclusions

- 1) When  $n=0.5$ , the filling gangue has smaller initial void and stronger resistance to deformation. If the volume compression is more than 10%, the filling of gangue has a certain bearing capacity. After the volume compression of 13%, the resistance of filling gangue to the deformation of surrounding rock is greater.

- 2) Under the condition of gangue filling, the direct roof is the cantilever beam structure after the first weighting, the moving fractured arch is formed around the overburden rock. With the compaction of filling gangue, the stress concentration around goaf decreases obviously.

- 3) Combining the equivalent mining height theory with the probability integration method, three allowable mining heights can be calculated and the maximum allowable mining height under the building is the minimum value, the full ratio and the ultimate strain are calculated and applied to the field.

### Data availability statement

All the data in this paper are available.

### Author contributions

All the authors contributed to publishing this paper.

C.W. and J.C. conceived the main idea of the paper; B.S. analyzed the data; C.W. and Y.Y.L. contributed theoretical analysis; C.W. wrote the paper; Wei.T, Zhe.J and Yin.L. did a lot work to modify figures and proofread the revised version.

## Acknowledgments

The research described in this paper was financially supported from the funding of the Shandong Provincial Doctoral Program for Overseas Studies, Taishan Scholar Talent Team Support Plan for Advantaged & Unique Discipline Areas and Key research and development plan of Shandong Province (2018GSF117018; 2018GSF120003; 2019GSF111024), Shandong Provincial Natural Science Foundation (ZR2019BEE013) and National Natural Science Foundation of China(51804179; 51604167; 51974173), State Key Laboratory of Mining Disaster Prevention and Control Co-founded by Shandong Province and the Ministry of Science and Technology(MDPC2016ZR01).

## Conflicts of interest

The authors declare no conflict of interest.

## References

- An, B., Miao, X., Zhang, J., Ju, F. and Zhou, N. (2016), "Overlying strata movement of recovering standing pillars with solid backfilling by physical simulation", *Int. J. Min. Sci. Technol.*, **26**(2), 301-307. <https://doi.org/10.1016/j.ijmst.2015.12.017>.
- Casini, F., Viggiani, G.M.B. and Springman, S.M. (2013), "Breakage of an artificial crushable material under loading", *Granul. Matter* **15**(5), 661-673. <https://doi.org/10.1007/s10035-013-0432-x>
- Chen, S.J., Yin, D. W., Jiang, N., Wang, F. and Guo, W.J. (2019), "Simulation study on effects of loading rate on uniaxial compression failure of composite rock-coal layer", *Geomech. Eng.*, **17**(4), 333-342. <https://doi.org/10.12989/gae.2019.17.4.333>.
- Coop, M.R., Sorensen, K.K., Freitas, T.B. and Georgoutsos, G (2004), "Particle breakage during shearing of a carbonate sand", *Geotechnique*, **54**(3), 157-163. <https://doi.org/10.1680/geot.2004.54.3.157>.
- Donohue, S., O'Sullivan, C. and Long, M. (2009), "Particle breakage during cyclic triaxial loading of a carbonate sand", *Géotechnique*, **59**(5), 477-482. <https://doi.org/10.1680/geot.2008.T.003>.
- Friedemann, J., Wagner, A., Heinze, A., Krzack, S. and Meyer, B. (2016), "Direct optical observation of coal particle fragmentation behavior in a drop-tube reactor", *Fuel*, **166**, 382-391. <https://doi.org/10.1016/j.fuel.2015.11.007>.
- Ghabchi, R., Zaman, M., Kazmee, H. and Singh, D. (2014), "Effect of shape parameters and gradation on laboratory-measured permeability of aggregate bases", *Int. J. Geomech.*, **15**(4), 04014070. [http://dx.doi.org/10.1061/\(ASCE\)GM.1943-5622.0000397](http://dx.doi.org/10.1061/(ASCE)GM.1943-5622.0000397)
- Gu, H., Tao, M., Wang, J., Jiang, H., Li, Q. and Wang, W. (2018), "Influence of water content on dynamic mechanical properties of coal", *Geomech. Eng.*, **16**(1), 85-95. <https://doi.org/10.12989/gae.2018.16.1.085>.
- Guida, G., Bartoli, M., Casini, F. and Viggiani, G.M. (2016), "Weibull distribution to describe grading evolution of materials with crushable grains", *Procedia Eng.*, **158**, 75-80. <https://doi.org/10.1016/j.proeng.2016.08.408>.
- Guo, G., Zhu, X., Zha, J. and Wang, Q. (2014), "Subsidence prediction method based on equivalent mining height theory for solid backfilling mining", *Trans. Nonferr. Metals Soc. China*, **24**(10), 3302-3308. [https://doi.org/10.1016/S1003-6326\(14\)63470-1](https://doi.org/10.1016/S1003-6326(14)63470-1).
- Guo, W. (2013), *Backfill Mining Technology in Coal Mines*, China Coal Industry Publishing House, Beijing, China.
- Guo, W., Gu, Q., Tan, Y. and Hu, S. (2019), "Case studies of rock bursts in tectonic areas with facies change", *Energies*, **12**(7), 1330. <https://doi.org/10.3390/en12071330>.
- Guo, W., Yu, F., Tan, Y. and Zhao, T. (2019), "Experimental study on the failure mechanism of layer-crack structure", *Energy Sci. Eng.*, 1-22. <https://doi.org/10.1002/ese3.407>.
- Hu, C., Wang, X., Mei, Y., Yuan, Y. and Zhang, S. (2018), "Compaction techniques and construction parameters of loess as filling material", *Geomech. Eng.*, **15**(6), 1143-1151. <https://doi.org/10.12989/gae.2018.15.6.1143>.
- Indraratna, B. and Locke, M.R (1999), "Design methods for granular filters-Critical review", *Geotech. Eng.*, **137**(3), 137-147. <https://doi.org/10.1680/gt.1999.370303>.
- Karacan, C.Ö. (2010), "Prediction of porosity and permeability of caved zone in longwall gobs", *Transp. Porous Media*, **82**, 413-439. <https://doi.org/10.1007/s11242-009-9437-7>.
- Kratzsch, I.H. (1983), "Mining subsidence engineering", *Environ. Geol. Water Sci.*, **8**(3), 133-136. <https://doi.org/10.1007/BF02509900>.
- Li, J., Huang, Y., Qiao, M., Chen, Z., Song, T., Kong, G., Gao, H. and Guo, L. (2018), "Effects of water soaked height on the deformation and crushing characteristics of loose gangue backfill material in solid backfill coal mining", *Processes*, **6**(6), 64. <https://doi.org/10.3390/pr6060064>
- Li, M., Zhang, J. and Gao, R. (2016), "Compression characteristics of solid wastes as backfill materials", *Adv. Mater. Sci. Eng.*, 2496194. <http://dx.doi.org/10.1155/2016/2496194>.
- Li, Y.Y., Zhang, S.C. and Zhang, X. (2018), "Classification and fractal characteristics of coal rock fragments under uniaxial cyclic loading conditions", *Arab. J. Geosci.*, **11**(9), 201-212. <https://doi.org/10.1007/s12517-018-3534-2>.
- Liu, X.S., Gu, Q.H., Tan, Y.L., Ning, J.G. and Jia, Z. (2019). "Mechanical Characteristics and Failure Prediction of Cement Mortar with a Sandwich Structure". *Minerals*, **9**(3), 143. <https://doi.org/10.3390/min9030143>
- Ma, D., Duan, H.Y., Liu, J.F., Li, X.B. and Zhou, Z.L. (2019), "The role of gangue on the mitigation of mining-induced hazards and environmental pollution: An experimental investigation", *Sci. Total Environ.*, **664**(10) 436-448. <https://doi.org/10.1016/j.scitotenv.2019.02.059>.
- Ma, D., Mohammad, R., Yu, H.S. and Bai, H.B. (2017), "Variations of hydraulic properties of granular sandstones during water inrush: Effect of small particle migration", *Eng. Geol.*, **217**(30) 61-70. <https://doi.org/10.1016/j.enggeo.2016.12.006>.
- Marcin, L. and Miguel, A. (2016), "Characteristics of carbon dioxide sorption in coal and gas shale-The effect of particle size", *J. Nat. Gas Sci. Eng.*, **28**, 558-565. <https://doi.org/10.1016/j.jngse.2015.12.037>.
- Muriithi, G.N., Petrik, L.F., Gitari, W.M. and Doucet, F.J. (2017), "Synthesis and characterization of hydrotalcite from South African Coal fly ash", *Powder Technol.*, **312**, 299-309. <https://doi.org/10.1016/j.powtec.2017.02.018>.
- Poulsen, B.A. and Adhikary, D.P. (2013), "A numerical study of the scale effect in coal strength", *Int. J. Rock Mech. Min. Sci.*,

- 63, 62-71. <https://doi.org/10.1016/j.ijrmms.2013.06.006>.
- Rozenblat, Y., Portnikov, D., Levy, A., Kalman, H., Aman, S. and Tomas, J. (2011), "Strength distribution of particles under compression", *Powder Technol.*, **208**(1), 215-224. <https://doi.org/10.1016/j.powtec.2010.12.023>.
- Shahriar, M.A., Sivakugan, N., Das, B.M., Urquhart, A. and Tapiolas, M. (2015), "Water table correction factors for settlements of shallow foundations in granular soils", *Int. J. Geomech.*, **15**(1), 06014015. [https://doi.org/10.1061/\(ASCE\)GM.1943-5622.0000391](https://doi.org/10.1061/(ASCE)GM.1943-5622.0000391).
- State Administration of Coal Industry (2017), *Regulations for the Preservation and Mining of Coal Pillars in Buildings, Water Bodies, Railways and Main Roadways*, Coal Industry Publishing House, Beijing, China.
- Sun, W., Du, H., Zhou, F. and Shao, J. (2019), "Experimental study of crack propagation of rock-like specimens containing conjugate fractures", *Geomech. Eng.*, **17**(4), 323-331. <https://doi.org/10.12989/gae.2019.17.4.323>.
- Talbot, A.N., Brown, H.A. and Richart, F.E. (1923). "The strength of concrete-its relation to the cement, aggregates and water", University of Illinois at Urbana Champaign, Illinois, U.S.A.
- Vogler, D., Amann, F., Bayer, P. and Elsworth, D. (2016), "Permeability evolution in natural fractures subject to cyclic loading and gouge formation", *Rock Mech. Rock Eng.*, **49**, 3463-3479. <https://doi.org/10.1007/s00603-016-1022-0>.
- Wang, C., Jiang, N., Shen, B., Sun, X., Zhang, B., Lu, Y. and Li, Y. (2019), "Distribution and evolution of residual voids in longwall old goaf", *Geomech. Eng.*, **19**(2), 105-114. <https://doi.org/10.12989/gae.2019.19.2.105>.
- Wang, C., Lu, Y., Li, Y., Zhang, B. and Liang, Y. (2019), "Deformation process and prediction of filling gangue: A case study in China", *Geomech. Eng.*, **18**(4), 417-426. <https://doi.org/10.12989/gae.2019.18.4.417>.
- Wang, H., Poulsen, B.A., Shen, B., Xue, S. and Jiang, Y. (2011), "The influence of roadway backfill on the coal pillar strength by numerical investigation", *Int. J. Rock Mech. Min. Sci.*, **48**(3), 443-450. <https://doi.org/10.1016/j.ijrmms.2010.09.007>.
- Yin, D., Chen, S. and Liu, X.Q. (2018), "Effect of joint angle in coal on failure mechanical behavior of roof rock-coal combined body", *Quart. J. Eng. Geol. Hydrogeol.*, **51**(2), 202-209. <https://doi.org/10.1144/qjegh2017-041>.
- Zhang, B. and Meng, Z. (2019), "Experimental study on floor failure of coal mining above confined water", *Arab. J. Geosci.*, **12**(4), 114-123. <https://doi.org/10.1007/s12517-019-4250-2>.
- Zhang, J., Li, B., Zhou, N. and Zhang, Q. (2016), "Application of solid backfilling to reduce hard-roof caving and longwall coal face burst potential", *Int. J. Rock Mech. Min. Sci.*, **88**, 197-205. <http://dx.doi.org/10.1016%2Fj.ijrmms.2016.07.025>.
- Zhang, Q., Zhang, J., Han, X., Ju, F., Tai, Y. and Li, M. (2016), "Theoretical research on mass ratio in solid backfill coal mining", *Environ. Earth Sci.*, **75**(7), 1-11. <https://doi.org/10.1007/s12665-015-5234-5>.
- Zhang, X., Lin, J., Liu, J., Li, F. and Pang, Z. (2017), "Investigation of hydraulic-mechanical properties of paste backfill containing coal gangue-fly ash and its application in an underground coal mine", *Energies*, **10**(9), 1309. <https://doi.org/10.3390/en10091309>.
- Zhao, J., Jiang, N. and Yin, L. (2019), "The effects of mining subsidence and drainage improvements on a waterlogged area", *Bull. Eng. Geol. Environ.*, **78**(5), 3815-3831. <https://doi.org/10.1007/s10064-018-1356-9>.
- Zhao, J., Yin, L. and Guo, W. (2018), "Stress-seepage coupling of cataclastic rock masses based on digital image technologies", *Rock Mech. Rock Eng.*, **51**(8), 2355-2372. <https://doi.org/10.1007/s00603-018-1474-5>.